Mutational analysis of the KIX domain of CBP reveals residues critical for SREBP binding

Ya-Ping Liu, Ching-Wen Chang, Kung-Yao Chang*

Institute of Biochemistry, National Chung-Hsing University, 250 Kuo-Kung Road, Taichung 402, Taiwan

Received 25 August 2003; revised 18 September 2003; accepted 18 September 2003

First published online 24 October 2003

Edited by Thomas L. James

Abstract Structure-based mutagenesis was used to probe the binding surface for the activation domain of sterol-responsive element binding protein (SREBP) in the KIX domain of CREB binding protein. A set of conserved residues scattering in the α2 helix and the extended C-terminal region of α3 helix in the KIX domain including two arginines previously characterized as a hot spot for cofactor-mediated methylation was shown to be crucial for SREBP–KIX interaction, and was not essential for phosphorylated KID recognition. Therefore, our results suggest the existence of a SREBP binding site formed by positively charged residues in the C-terminal part of the extended α3 helix of the KIX domain distinct from the previously identified phosphorylated KID binding site.

Key words: Sterol-responsive element binding protein; cAMP-responsive element binding protein; CREB binding protein; Structure-based mutagenesis; Protein–protein interaction; Post-translational modification

1. Introduction

The cAMP-responsive element binding protein (CREB) binding protein (CBP) and p300 belong to a family of bridging proteins serving as general transcription co-activators with intrinsic acetyltransferase activity [1–3]. They can connect many DNA binding factors to the basal transcription machinery via direct protein–protein interactions with the activation domain of transcription factors, and present histone acetyltransferases to specific nucleosomes containing the target gene promoters to play roles in chromosome remodeling [4,5]. Interactions between CBP/p300 and transcriptional activators are mediated by several conserved docking domains in the both ends of CBP/p300. Among them, the KIX domain is located in the N-terminal part of CBP/p300 and has been shown to be responsible for the recruitment of at least a dozen transcription factors [3,6–11]. For example, the KIX domain of CBP/p300 can recruit CREB by associating with the serine 133-phosphorylated KID domain of CREB to activate CRE-bearing gene expression in response to cAMP signals [2,6]. On the other hand, other transcription factors, such as c-Myb, Jun, sterol-responsive element binding protein (SREBP) and the activation domain of mixed lineage leukemia (MLL) protein, interact with the KIX domain in a constitutive way without the need for phosphorylation by kinases [7–11]. Sequence alignment of these factors revealed no consensus KIX recognition motif among them [12,13]. An interesting question is thus how the KIX domain recognizes so many transcription factors of different natures.

The structure of the pKID–KIX complex has been solved [14,15]. It shows the structure of the pKID-bound KIX is composed of three mutually interacting helices, α1, α2 and α3 with two short bridging 3_{10} helices, G1 and G2. The pKID binding surface in the KIX domain is formed by a hydrophobic groove constituted by the α1 and α3 helices. Mutagenesis studies of the KIX domain implicated the same hydrophobic groove as the major binding site for both CREB and c-Myb [12], and were recently confirmed by nuclear magnetic resonance (NMR) studies [16]. No obvious sequence similarity could be found in the regions responsible for KIX binding by CREB and c-Myb although the spacing patterns of critical hydrophobic residues in these regions are similar [12]. Phage display selection of small peptides capable of competing with pKID for KIX domain binding also revealed a similar spacing pattern of amphipathic nature [17]. Together with the results of thermodynamic analysis for the binding processes of CREB and c-Myb toward the KIX domain, it was proposed that the KIX domain bound an amphipathic helix formed by either the pKID of CREB or the activation domain of c-Myb although the mechanisms underlined the binding was different between these two ligands [12,16]. However, recent NMR chemical shift mapping analysis of the MLL-bound and p-Jun-bound KIX indicated the existence of a distinct binding surface for MLL and p-Jun recognition in addition to the amphipathic helix binding surface for CREB docking [18,19]. It thus raises the possibility that there exist distinct ligand binding pockets for other KIX binding ligands [18,19]. In this work, structure-based mutagenesis in combination with in vitro binding assays will be used to show different sets of residues in the KIX domain of CBP are essential for CREB and SREBP binding respectively. Furthermore, two conserved arginines required for SREBP binding identified in this work may participate in a recently explored post-translational modification circuit that could lead to the regulation of SREBP-mediated gene expression.

2. Materials and methods

2.1. Plasmids

The genes encoding the KIX domain of human CBP (KIX_{98}, containing residues 586–683), the KID domain of human CREB (KID_{60}, containing residues 86–145) and the minimal KIX binding region of

*Corresponding author. Fax: (886)-4-22853487.
E-mail address: kychang@dragon.nchu.edu.tw (K.-Y. Chang).

0014-5793/03/$22.00
doi:10.1016/S0014-5793(03)01200-6

human SREBP ($SREBP_{29}$, containing residues 17–45) were constructed by a polymerase chain reaction (PCR)-based ligation approach [20]. Each gene was assembled from different pieces of chemically synthesized DNA oligonucleotides that cover the open reading frame of the gene of interest. Long partially overlapping oligonucleotides with sequences taken from both strands of the gene of interest were designed and the DNA sequences in some codons were changed to encode the favored codons used in bacteria to facilitate expression (see Table 1 for the designed DNA sequences used in the PCR-based ligation). Recombinant expression vectors for KID_{60} and $SREBP_{29}$ were obtained by sub-cloning the gene fragments obtained from PCR-based ligation into the *Bam*HI/*Eco*RI sites of the pGEX-4T1 expression vector (Pharmacia). These recombinant pGEX-KID_{60} and pGEX-$SREBP_{29}$ were then used to express glutathione *S*-transferase (GST)-KID_{60} and GST-$SREBP_{29}$ fusion proteins used in the GST pull-down assay. The pMal-c2x expression vector (New England Biolabs) was used as the vehicle for the construction of expression vector for myelin basic protein (MBP)-KIX_{98} fusion protein. A blue-white screen procedure was performed to identify TB1 colonies carrying an insert with the desired KIX_{98} gene according to the instructions of the manufacturer. The recombinant pMal fusion vectors were then recovered and retransformed into competent BL21 (DE3) cells for MBP-KIX_{98} protein expression after sequence verification. All the mutants with point mutation in KIX_{98} were created using the QuickChange site-directed mutagenesis kit (Stratagene) according to the manufacturer's instructions with appropriate primers (the sequences are available upon request). The identities of all cloned and mutated genes were confirmed by DNA sequencing analysis.

2.2. Expression and purification of fusion proteins

Escherichia coli BL21 (DE3) cells were used as the host for the expression of GST-tagged and MBP-tagged fusion proteins. The transformed bacteria were grown in LB medium (enriched with 0.2% mM glucose for expressing MBP-tagged protein) in the presence of 100 μg/ml ampicillin to an A^{600} value of 0.6–0.8 at 37°C. Expression of proteins was then induced by the addition of 1 mM isopropyl-1-thio-β-D-galactopyranoside (IPTG) and the growth of cells was continued for another 2 or 3 h for MBP-tagged or GST-tagged proteins respectively. The cells were then collected by centrifugation and suspended in phosphate-buffered saline (PBS) buffer (10 mM Na_2HPO_4, 1.8 mM KH_2PO_4, 140 mM NaCl, 2.7 mM KCl, 0.2 mM phenylmethylsulfonyl fluoride (PMSF), pH 7.3) for storage at −80°C.

For the purification of expressed proteins, the frozen cell pellets containing expressed GST fusion proteins were thawed and sonicated in the presence of 1 mM PMSF. The cell lysates were centrifuged and the clarified lysates were then applied into a pre-packed glutathione-agarose bead column (Pharmacia) equilibrated with PBS buffer. After extensive washing with 25 column volumes of PBS buffer, the GST-tagged proteins were eluted with 1 column volume of elution buffer of 50 mM Tris–HCl and 10 mM reduced glutathione at pH 8.0. The fractions containing eluted fusion proteins (checked by sodium dodecyl sulfate–polyacrylamide gel electrophoresis (SDS–PAGE) and Coomassie brilliant blue staining) were pooled and dialyzed against buffer containing 10 mM Na_2HPO_4, 10 ng/ml pepstatin and 1 mM PMSF of pH 8.0 for 12 h at 4°C and stored as separate aliquots at −80°C. The protein purity was examined by SDS–PAGE, while the protein concentration was measured using the Bradford assay (Bio-Rad). The phosphorylation of KID_{60} was performed on the GST-KID_{60} fusion protein in the presence of protein kinase A (Pharmacia) using the conditions described by Parker et al. [6].

2.3. GST pull-down assay

The GST fusion proteins used in the pull-down assay were purified as described above and about 15 μg of GST-pKID_{60} or 35 μg of GST-$SREBP_{29}$ was used for each pull-down reaction. The input levels of MBP-KIX_{98} and MBP-KIX_{98} mutants within the cell extracts were checked using SDS–PAGE by comparing with pre-purified standard calibrated by the Bradford assay, and were estimated to be around 50 μg per reaction. Cell extracts expressing MBP-KIX_{98} or its mutants were incubated with GST-, GST-pKID_{60}- or GST-$SREBP_{29}$-bound beads in binding buffer (20 mM HEPES, pH 7.5, 150 mM NaCl, 1 mM EDTA, 1 mM dithiothreitol, 0.1% PMSF and 10% glycerol) for 90 min at 4°C. The beads were then washed five times with ice-cold binding buffer, and the complex-containing beads were re-suspended in 2×SDS loading buffer and resolved by 12% SDS–PAGE. The resolved protein bands were visualized by either Coomassie brilliant blue staining or Western blotting following a standard procedure using anti-MBP antibody (Santa Cruz Biotechnology). All the GST pull-down experiments for each mutant were performed at least three times with the same conclusion.

2.4. Quantitative analysis of in vitro binding efficiency

The amount of protein pulled down in the GST pull-down experiment can be calculated by analyzing the resolved protein bands on SDS–PAGE stained with Coomassie brilliant blue. To do so, the intensity of each stained protein band was scanned and measured by an infrared imaging system, Odyssey (Li-Cor), and compared with that of a standard to estimate the quantity of the protein in the band of interest. The accuracy of this approach was first confirmed using a bovine serum albumin (BSA) standard calibrated by the Bradford assay. Purified GST fusion proteins were calibrated with the BSA standard to make a stock solution of 1 μg/μl and samples of a series of diluted GST fusion protein were then analyzed by SDS–PAGE. After being extensively destained by the destaining solution after Coomassie brilliant blue treatment, the gel was scanned by the imaging system to record the intensity of each band. The results were then analyzed by Odyssey imager software and compared with the theoretical dilution factor as well as the result obtained in the Bradford assay. A good correlation between the theoretical dilution factor and the calculated factor from Odyssey analysis was obtained for a dilution factor of 10 for protein quantities in the range of 0.2–2 μg.

To evaluate the effect of each KIX_{98} mutant on binding of either GST-pKID_{60} or GST-$SREBP_{29}$, the binding efficiency of each KIX_{98} mutant toward pKID_{60} or $SREBP_{29}$ was calculated by analyzing the SDS–PAGE gel used to resolve the eluted bound proteins in the GST pull-down experiment as described in Section 2.3. The measured intensity of a protein band corresponding to a specific KIX_{98} mutant was divided by that corresponding to the wild-type KIX_{98} control resolved in the same gel to get a relative binding ratio for each KIX_{98} mutant. As can be seen, variation occurs among wild-type and mutant KIX_{98} for the eluted GST fusion protein detected in the SDS–PAGE gel. To calibrate this variation, the amount of the GST fusion protein co-eluted with a specific KIX_{98} mutant was divided by that co-eluted with the wild-type KIX_{98} resolved in the same gel to get a normalization factor for each mutant. We then divided the relative binding ratio by the normalization factor for each mutant to

Table 1
The sequences for the designed DNA oligonucleotides used to construct the genes encoding $CBP_{586-683}$/KIX_{98}, $CREB_{101-160}$/KID_{60}, and $SREBP_{17-45}$/$SREBP_{29}$ by PCR-based ligation

KIX-1	5′-CCGAGAATTCACTGGTGTACGCAAAGGCTGGCATGAACACGTAACTCAGGACCTTCGTAGCCATCTGGT-3′
KIX-2	5′-TGAGAGCTGCTGGATCTGGAGTCGGGAAGATTGCTTGTACCAGTTTGTGTACCAGATGGCTACGAAGGTC-3′
KIX-3	5′-TCCAGATCCAGCAGCTCTCAAGGATCGTCGCATGGAGAACCTGGTAGCGTATGCTAAGAAAGTGGAGGGC-3′
KIX-4	5′-TGCGAGCAGGTGATAGTATTCATCACGGGAGTTCGCAGACTCGTACATATCGCCCTCCACTTTCTTAGCAT-3′
KIX-5	5′-GAATACTATCACCTGCTCGCAGAGAAGATTTACAAGATTCAGAAGAACTGGAAGAGAAACGCCGTTCTC-3′
KIX-6	5′-CCGATTCTCGAGTCATGGCTGGTTGCCCAGGATGCCTTGCTTATGCAGACGAGAACGGCGTTTCTCTTCC-3′
KID-1	5′-CGATGCACATATGCAGATTTCTACTATCGCAGAATCCGAGGATAGCCAGGAGTCCGTAGACTCCGTT-3′
KID-2	5′-TAGCTCGGGCGACGAGACAGGATCTCACGGCGTTTCTGAGAATCGGTAACGGAGTCTACGGACTCCTGG-3′
KID-3	5′-CTGTCTCGTCGCCCGAGCTACCGCAAGATCCTGAACGACCTGTCCTCTGACGCACCAGGTGTACCAC-3′
KID-4	5′-GTATTCGGATCCTTAGGTTTCCTCTTCAGACTTTTCTTCCTCGATACGTGGTACACCTGGTGCGTCA-3′
SREBP-1	5′-TAGCGTGGATCCGAACTGGGTGAGCTGGACGCAGCTCTGCTGACCGACATCGAAGATATGCTCCAAC-3′
SREBP-2	5′-CAGGGAATTCAGCTAACCTGGGAAGTCGGAATCCTGGTTGTTAATCAGTTGGAGCATATCTTCGATGT-3′

get the final binding efficiency of each KIX_{98} mutant, presented as a percentage of the value of wild-type KIX_{98} with the wild-type value set at 100. During this calculation, we assumed that all KIX_{98} mutants and the wild-type KIX_{98} have the same molecular weight.

2.5. Three-dimensional model mapping

The results of binding efficiency analysis for each KIX_{98} mutant were mapped into the 3D model of a KIX domain built upon the published pKID-bound KIX structure [14]. A mutated residue that resulted in a mutant with a binding efficiency below 30% of that of the wild-type KIX_{98} was assigned as essential for binding, whereas those that fell between 30% and 60% were assigned to be critical for binding. The 3D model containing 90 residues (residues 587–676) was generated based on the published mouse KIX domain structure [14] using the program O [21]. Because the atomic coordinates for the C-terminal residues from 668 to 676 are not available from the published structure, residues 668–671 were modeled as an extension of the α3 helix to adopt the helical conformation as reported [15]. Since no information on the local conformation is available for residues 672–676, this region was thus modeled as a coil. No molecular dynamic simulation was applied to this model.

3. Results

3.1. Comparison of the minimal region responsible for KIX binding in SREBP with those in CREB and c-Myb reveals both similar and different features

Sequence comparison of the minimal domains required for

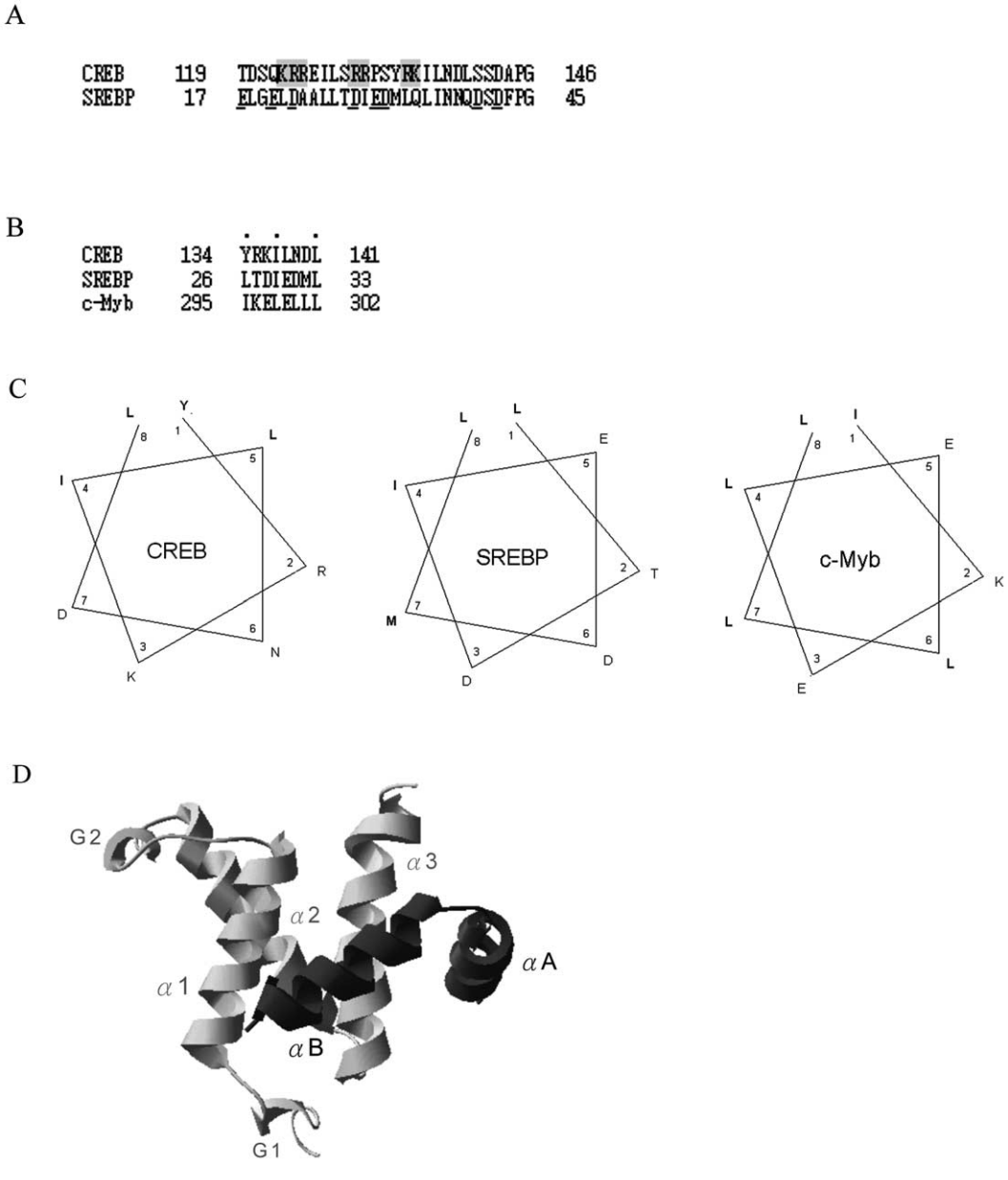

Fig. 1. Comparison of the regions required for KIX binding between CREB and SREBP. A: Sequence alignment for the minimal KIX binding regions of CREB and SREBP shows a dramatic difference in the nature of the charge for the polar side chains. Positively charged residues are shaded while negatively charged residues are underlined. B: Conserved hydrophobic residues (labeled with dots on the top) with a fixed spacing pattern can be found for the regions required for KIX binding in CREB, c-Myb and SREBP. C: Helical wheel prediction indicates the existence of a predicted amphipathic helix for the KIX binding regions of CREB, SREBP and c-Myb respectively. D: A ribbon diagram of the NMR structure of the KIX–pKID complex [14] with the conserved hydrophobic groove for CREB docking formed by the parallel α1 and α3 helices of KIX facing the viewer. The gray ribbons represent the KIX domain while the black ribbons belong to pKID with their constituent secondary structures shown as indicated.

KIX binding between SREBP, KID and c-Myb indicated a dramatic difference in the nature of the charge for the polar side chains between $CREB_{119-146}$ and $SREBP_{17-45}$. Two thirds of the polar side chains in $CREB_{119-146}$ are positively charged, whereas there are only negatively charged ones in $SREBP_{17-45}$ (Fig. 1A). On the other hand, the spacing of the conserved hydrophobic residues does show a similar pattern among the KIX binding regions of CREB, SREBP and c-Myb, suggesting they may dock into the same hydrophobic groove in KIX (Fig. 1B,C). However, mutational studies on SREBP indicated that some interactions important for pKID–KIX recognition were not required for SREBP–KIX interaction although the hydrophobic residues did contribute to the binding [22]. Furthermore, replacement of the key residues in KID involving direct KIX binding with a stretch of six non-conserved residues, DIEDML in SREBP, led to the formation of a chimeric KID capable of binding CBP with high affinity, suggesting the binding mechanisms of pKID and SREBP to KIX might not be identical [22]. Finally, circular dichroism spectroscopy of the minimal KIX binding region of SREBP, $SREBP_{29}$, revealed a random coil content similar to that of KID (data not shown), and very different from the reported 30% helical content for c-Myb although both SREBP and c-Myb bound to KIX in a phosphorylation-independent way

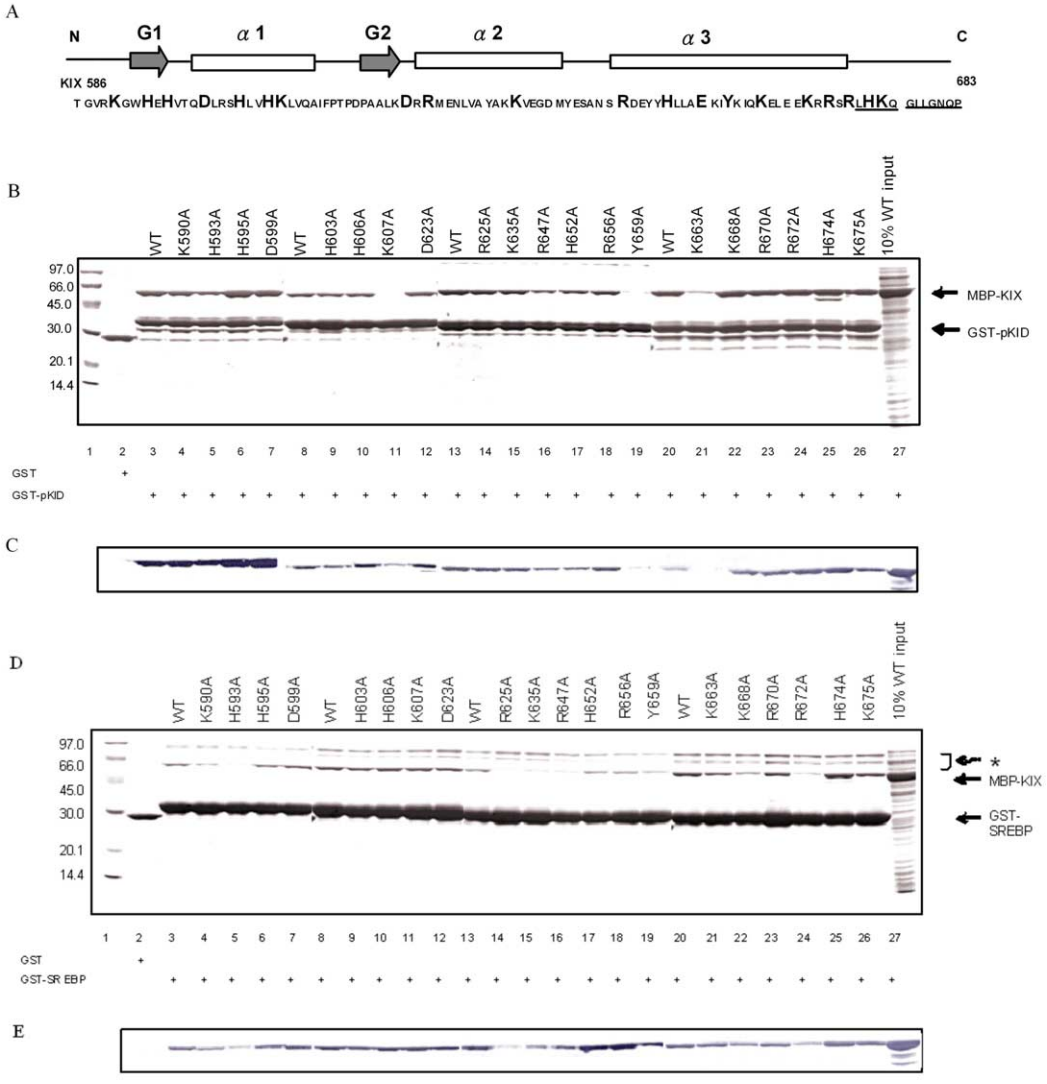

Fig. 2. In vitro binding assay of GST-$pKID_{60}$ and GST-$SREBP_{29}$ toward wild-type and mutant KIX_{98}. A: Schematic representation of KIX_{98} with the residues mutated for study in bold. Please note that this construct contains 11 extra residues in the C-terminal end (these residues are underlined) compared with the construct derived from mouse CBP used for NMR study [15]. Since there is a one-residue shift between the mouse and human KIX, residue 625 in this KIX_{98} construct will thus correspond to residue 624 in the NMR construct and the numbering difference is also applicable to all the other residues. B: Results of 12% SDS–PAGE for GST pull-down assay between GST-$pKID_{60}$ and MBP-KIX_{98} variants (as indicated at the top of each well) stained with Coomassie brilliant blue. The smaller fragments below GST-$pKID_{60}$ belong to degraded products of GST-$pKID_{60}$. C: Western blotting result for B using the antibody against MBP. D: Results of 12% SDS–PAGE analysis for GST pull-down assay between GST-$SREBP_{29}$ and MBP-KIX_{98} variants (as indicated at the top of each well) stained with Coomassie brilliant blue. The bands at the top of the gel with a dashed arrow correspond to the dimerized GST fusion protein as revealed by Western blotting using anti-GST antibody (data now shown). E: Western blotting result for D using the antibody against MBP. All the GST pull-down experiments for each mutant were performed at least three times with the same conclusion.

[12]. Together, these results prompted us to examine if the KIX domain uses the same pKID binding surface to recognize SREBP.

3.2. Mutations in key residues in the KIX domain involving direct contact with pKID lead to a dramatic loss of pKID binding efficiency in the in vitro binding assay

Structure-based mutagenesis provides a rational way to design mutants for functional studies because it helps avoid mutants with global conformational change that can generate data difficult to interpret. Up to date, there is no structural information available for the interaction between SREBP and KIX. With the pKID–KIX complex structure (Fig. 1D), we reasoned that a parallel comparison of the binding efficiency between phosphorylated KID and SREBP toward wild-type and mutants of the KIX domain using an in vitro binding assay should provide valuable information regarding the recognition of SREBP by the KIX domain. Therefore, we created a series of KIX mutants using the published KIX–pKID complex structure as a guide to avoid mutants that might impair the formation of the hydrophobic core of KIX. Several residues known to contact the pKID directly and other conserved residues on the surface of KIX were the major targets of mutagenesis. In total, we obtained 20 different point mutants of a 98-residue KIX domain derived from human CBP, KIX_{98} (Fig. 2A) that can be expressed successfully with a reasonable yield. All these KIX mutants were expressed as fusion proteins with a MBP tag in the N-terminal end to facilitate characterization by Western blotting using the antibody against MBP.

We then used a KID domain derived from human CREB, KID_{60}, as a test to examine the effects of different KIX_{98} mutants on $pKID_{60}$ binding and compared the results with the published complex structure and mutagenesis studies [12–15] with focus on mutants with reduced binding affinity. As shown in Fig. 2B,C, the KIX_{98} mutants for three key residues in the KIX domain involving CREB binding (K607A, Y659A and K663A) [13,14] all show dramatically reduced amounts of pulled-down products compared with the wild-type KIX_{98} against the phosphorylated GST-KID_{60}. Particularly, the reduced binding ability of mutant K663A, which was reported to have a 25-fold decrease in pKID binding affinity compared with the wild-type KIX, might not be fully appreciated, but it can be easily identified in our system [13,14]. In addition, five KIX_{98} mutants with reduced $pKID_{60}$ binding affinity are new from this study. Among them, the results for H603A, R647A and H652A can be explained as the result of mutation in residues directly contacting pKID based on the analysis of the published NMR structure. On the other hand, the observed reduction in $pKID_{60}$ binding for mutants K590A and H593A of KIX_{98} is probably caused by perturbation of intramolecular contacts within KIX. In the published structure, H593 was found to interact with R589 in stabilizing the G1 helix, whereas K590 could interact with S643 and N645 in the loop between the α2 and α3 helices of KIX to help organize their relative orientation. Mutation of H593 and K590 in the G1 region may thus perturb the local conformations that eventually lead to the reconfiguration of the CREB docking surface. Interestingly, most of the remaining KIX_{98} mutants resulted in an increase of binding affinity for $pKID_{60}$. Together, these results indicate a good correlation between the direct contact residues and the impairment of efficient $pKID_{60}$ binding in our assay, arguing that this approach can be used to search for critical residues in the KIX domain involving ligand binding.

3.3. Mutants on the surface of KIX with severe impairment of SREBP binding are mapped to a distinct region of the CREB docking site

We then applied the same procedure to look for the mutations on KIX that lead to an impairment of efficient $SREBP_{29}$ binding; the results are presented in Fig. 2D,E. In comparing

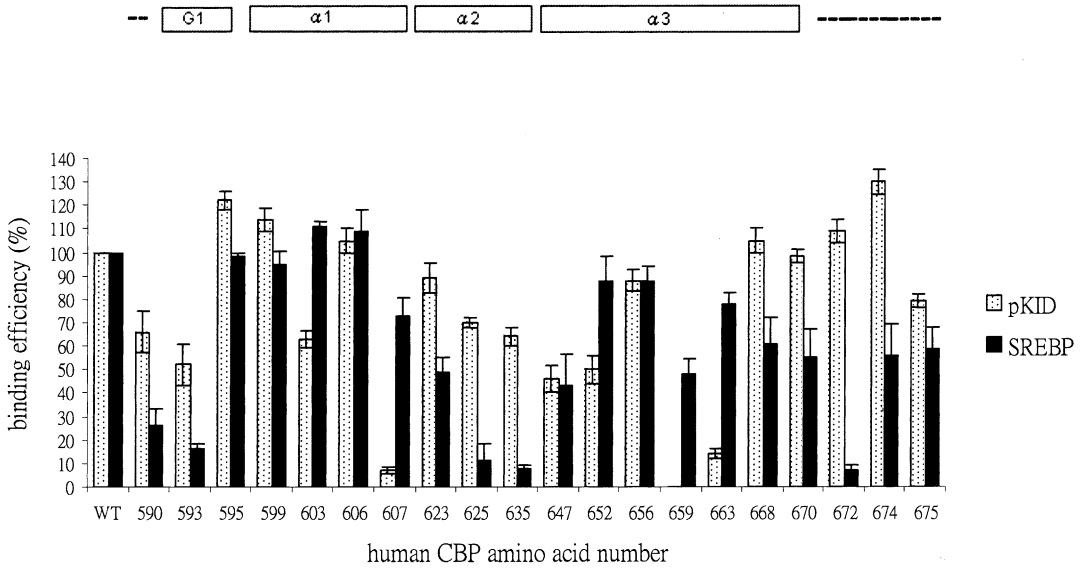

Fig. 3. Evaluation of the binding efficiency for different KIX_{98} mutants against $pKID_{60}$ and $SREBP_{29}$. The calculated GST-$pKID_{60}$ (striped bars) and GST-$SREBP_{29}$ (filled bars) binding efficiency of different MBP-KIX_{98} mutants compared with the wild-type MBP-KIX $_{98}$ is presented. The ligand binding efficiency of wild-type KIX_{98} is set as 100% and the schematic secondary structures that each mutated residue belongs to are shown at the top. The data were analyzed by performing volume integration of the bands corresponding to the pulled-down MBP-KIX_{98} variants, GST-$pKID_{60}$ and GST-$SREBP_{29}$, using the Odyssey imaging system (Li-Cor) and analyzed by Odyssey software with procedures described in Section 2. The plotted values are the means of three independent experiments, and the error bars are S.D.

the results with those from the KID_{60} binding assay (Fig. 2B,C), a broader distribution of KIX_{98} mutants with strongly affected SREBP binding ability is observed. Importantly, the mutated residues with severe impairment in $SREBP_{29}$ binding efficiency (R625A, K635A and R672A) do not overlap with those residues essential for the binding of $pKID_{60}$ (K607A, Y659A and K663A). It thus provides compelling evidence that residues directly contacting pKID do not appear to perform an essential role in the interaction with SREBP. Among the three residues crucial for SREBP binding, R672 in the C-terminal end of the extended α3 helix was previously thought to play a role, together with other positively charged residues nearby, in the stabilization of the hydrophobic core by neutralizing the negative helix dipole with their positively charged side chains [15]. Our results thus assign this conserved residue an extra role in the interaction with SREBP. Most interestingly, this R672 and the R625 in the N-terminal end of the α2 helix were also found to be the favored targets for post-translational methylation by CARM1 in a recent study [23]. Therefore, a possible transcriptional switch similar to that for CREB mediated by cofactor methylation may also exist for SREBP.

To further evaluate the effects of each KIX_{98} mutant on $pKID_{60}$ and $SREBP_{29}$ binding, we quantified the impact of each mutant on ligand binding by comparing the amount of bound KIX_{98} mutant with bound wild-type KIX_{98} toward a normalized amount of $pKID_{60}$ or $SREBP_{29}$ (see Section 2 for details). As shown in Fig. 3, the residues critical for pKID binding are clustered in the α1 helix and the N-terminal part of the α3 helix. In contrast, the residues important for SREBP binding are located in the α2 helix and the extended C-terminal region of the α3 helix. We also noticed that K590 and H593 in the G1 region of KIX exhibit a dramatic reduction in SREBP binding efficiency. However, a substantial reduction in pKID binding was also observed for mutation on these two residues. As K590 and H593 may participate in the intramolecular interactions that organize the tertiary fold of KIX as mentioned in Section 3.2, this impairment in ligand binding efficiency may thus be an indirect outcome of the disruption of critical tertiary interactions caused by mutation. Consistent with this interpretation, no intermolecular contact between the G1 region of KIX and pKID can be observed in the published complex structure [14]. We then mapped these results into a modified 3D structure of pKID-bound KIX to generate structural models displaying the critical regions involving $pKID_{60}$ or $SREBP_{29}$ binding respectively (Fig. 4). In the structural model, K607, Y659 and K663, which are essential for pKID binding, are mapped to the parallel α1 and α3 helices that form the CREB docking groove (Fig. 4A). On the other hand, the residues most critical for SREBP binding, that

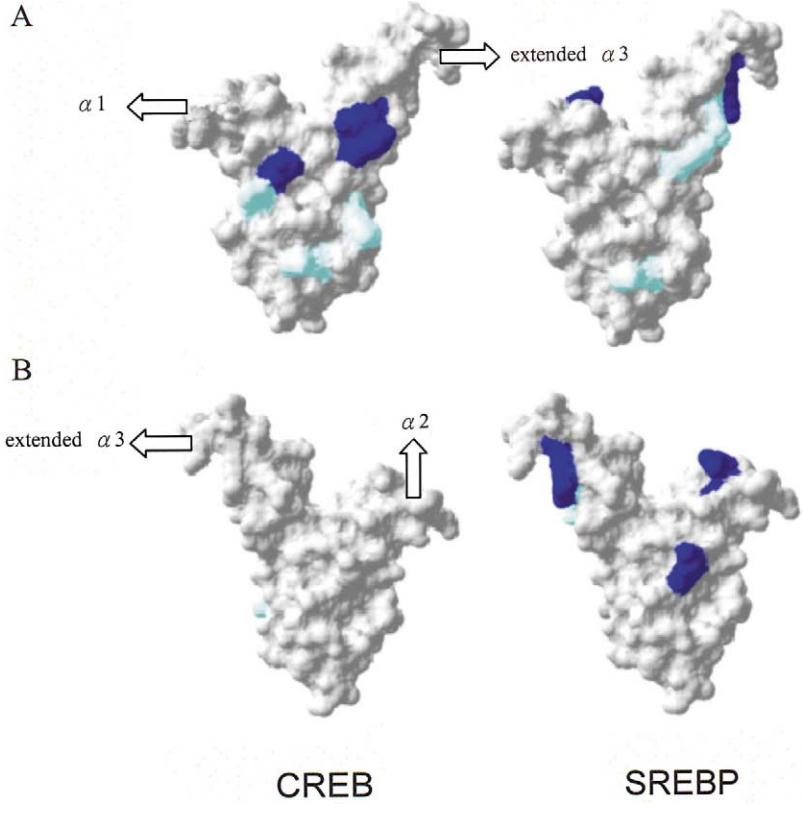

Fig. 4. Structural models for the location of KIX residues critical for SREBP binding. A: Models showing the parallel α1 and α3 helices of KIX that form the CREB docking groove with the residues critical for $pKID_{60}$ (left) and $SREBP_{29}$ binding (right) mapped into the models. This view is the same as that in Fig. 1D except that pKID is removed and extra residues are added to the C-terminal end of KIX. B: Models showing the surface formed by the α2 helix of KIX (turned 180° from the view in A) with the residues critical for $pKID_{60}$ (left) and $SREBP_{29}$ binding (right) mapped into the models. Residues that lead to a reduction of binding efficiency upon mutation are assigned to be essential for binding if the binding efficiency falls below 30% of that of the wild-type KIX and are shown in dark blue. In contrast, residues are assigned as critical for binding if the binding efficiency falls between 30% and 60% of that of the wild-type KIX; they are shown in light blue color. (For interpretation of the references to color in this figure legend, the reader is referred to the web version of this article.)

is, R625 and K635 in the α2 helix and R672 in the α3 helix, are located on the opposite side of the conserved hydrophobic groove for CREB docking, arguing for the existence of a distinct binding surface for SREBP (Fig. 4B).

4. Discussion

As part of efforts to elucidate the molecular mechanisms for the versatile transcriptional activator binding activity of the KIX domain of CBP, we used structure-based mutagenesis in combination with in vitro binding assays to probe the SREBP recognition surface of KIX. Since all the mutants that lose most of their SREBP binding abilities retain substantial CREB binding affinity, it is unlikely that the observed reduction in SREBP binding ability is caused by global mis-folding of the mutants. Our results thus clearly demonstrate that the pools of residues essential for CREB and SREBP binding are different, implying distinct binding sites in the KIX for these two transcription activators. Particularly, the positively charged residues located in the C-terminal region of the α3 helix represent a unique binding surface for SREBP (see the upper left corner in the right panel of Fig. 4B) as they have been shown to be dispensable for phosphorylated KID binding [15]. Together with R625 in α2 helix (the upper right corner in the right panel of Fig. 4B), this patch of positively charged residues can potentially gate the groove that is encircled by the extended α3 helix and the N-terminal part of the α2 helix although the conformation of the extended α3 helix remains unknown. However, we cannot rule out the possibility of overlap between the binding sites for pKID and SREBP due to the limitation in resolution because the numbers of mutants are not exhaustive. Besides, the local conformations for SREBP-bound KIX may be different from those for pKID-bound KIX that we know. Furthermore, residues in the α2 helix region (R625 and K635) do show some minor effects on $pKID_{60}$ binding although they appear to be absolutely required for $SREBP_{29}$ binding, whereas Y659, crucial for pKID binding, also affects the binding of SREBP substantially, implying a dual role for these residues in the recognition of both ligands. Intriguingly, we also noticed overlap between residues critical for SREBP binding in our studies and the residues involving MLL and p-Jun binding probed by NMR chemical shift mapping analysis [18]. For example, R625, crucial for SREBP binding, also exhibits a large chemical shift change upon the formation of MLL–KIX or p-Jun–KIX complex [18,19]. The NMR mapping results also indicated that residues scattered around G2 possessed the biggest chemical shift perturbation upon addition of MLL or p-Jun. Unfortunately, the number of available mutants (D623 and R625) in this region is limited in our study and it will await the 3D structure of the complex between SREBP and KIX to resolve these in detail.

As mentioned earlier, a major difference between KID and SREBP in sequence identity is the opposite nature of the charge of the side chains. The existence of a group of positively charged side chains essential for SREBP binding thus raises the possibility that electrostatic interactions may play an important role in the interaction between SREBP and KIX. However, the elucidation of the nature of this interaction will need more work. Finally, the finding that both R625 and R672 are hot spots for CARM1 methylation [23] may deserve further investigation because a post-translational modification by CBP with lysine acetylation in the DNA binding domain of SREBP has also been reported recently [24]. Since this acetylation can lead to the stabilization of SREBP, a modification by methylation of arginine residues critical for CBP–SREBP interaction may thus serve to regulate the metabolism of SREBP post-translationally.

Acknowledgements: We are very grateful to Dr. Hung-Wen Chen and Dr. Nei-Li Chan for useful comments and discussions on this work and to Dr. Nei-Li Chan for help in model building. This work was supported by Grant NSC 91-2311-B-005-038 from the National Science Council of Taiwan.

References

[1] Kwok, R.P.S., Lundblad, J.R., Chrivia, J.C., Richards, J.P., Bächinger, H.P., Brennan, R.G., Roberts, S.G.E., Green, M.R. and Goodman, R.H. (1994) Nature 370, 223–226.
[2] Lundblad, J.R., Kwok, R.P.S., Laurance, M.E., Harter, M.L. and Goodman, R.H. (1995) Nature 374, 85–88.
[3] Vo, N. and Goodman, R.H. (2001) J. Biol. Chem. 276, 13505–13508.
[4] Bannister, A. and Kouzarides, T. (1996) Nature 384, 641–643.
[5] Ogryzko, V., Schiltz, R., Russanova, V., Howard, B. and Nakatani, Y. (1996) Cell 87, 953–959.
[6] Parker, D., Ferreri, K., Nakajima, T., Lamorte, V.J., Evans, R., Koerber, S.S., Hoeger, C. and Montminy, M.R. (1996) Mol. Cell. Biol. 16, 694–703.
[7] Dai, P., Akimaru, H., Tanaka, Y., Hou, D.X., Yasukawa, T., Kanei-Ishii, C., Takahashi, T. and Ishii, S. (1996) Genes Dev. 10, 528–540.
[8] Lee, J.S., See, R.H., Deng, T. and Shi, Y. (1996) Mol. Cell. Biol. 16, 4312–4326.
[9] Bannister, A.J., Oehler, T., Wilhelm, D., Angel, P. and Kouzarides, T. (1995) Oncogene 11, 2509–2514.
[10] Oliner, J.D., Andresen, J.M., Hansen, S.K., Zhou, S. and Tjian, R. (1996) Genes Dev. 10, 2903–2911.
[11] Ernst, P., Wang, J., Huang, M. and Goodman, R.H. (2001) Mol. Cell. Biol. 21, 2249–2258.
[12] Parker, D., Rivera, M., Zor, T., Henrion-Caude, A., Radhakrishnan, I., Kumar, A., Shapiro, L.H. and Wright, P.E. (1999) Mol. Cell. Biol. 19, 5601–5607.
[13] Parker, D., Jhala, U.S., Radhakrishnan, I., Yaffe, M.B., Reyes, C., Shulman, A.I., Cantley, L.C., Wright, P.E. and Montminy, M. (1998) Mol. Cell 2, 353–359.
[14] Radhakrishnan, I., Pérez-Alvarado, G.C., Parker, D., Dyson, H.J., Montminy, M.R. and Wright, P.E. (1997) Cell 91, 741–752.
[15] Radhakrishnan, I., Pérez-Alvarado, G.C., Parker, D., Dyson, H.J., Montminy, M.R. and Wright, P.E. (1999) J. Mol. Biol. 287, 859–865.
[16] Zor, T., Mayr, B.M., Dyson, H.J., Montminy, M.R. and Wright, P.E. (2002) J. Biol. Chem. 277, 42241–42248.
[17] Frangioni, J.V., LaRiccia, L.M., Cantley, L.C. and Montminy, M.R. (2000) Nat. Biotechnol. 18, 1080–1085.
[18] Goto, N.K., Zor, T., Mattinez-Yamout, M., Dyson, H.J. and Wright, P.E. (2002) J. Biol. Chem. 277, 43168–43174.
[19] Campbell, K.M. and Lumb, K.J. (2002) Biochemistry 41, 13956–13964.
[20] Casimiro, D.R., Toy-Palmer, A., Blake II, R.C. and Dyson, H.J. (1995) Biochemistry 34, 6640–6648.
[21] Jones, T.A., Bergdoll, M. and Kjeldgaard, M. (1990) in: Crystallographic and Modeling Methods in Molecular Design (Bugg, C. and Ealick, S., Eds.), pp. 189–195, Springer-Verlag, New York.
[22] Cardinaux, J.R., Notis, J.C., Zhang, Q., Vo, N., Craig, J.C., Fass, D.M., Brennan, R.G. and Goodman, R.H. (2000) Mol. Cell. Biol. 20, 1546–1552.
[23] Xu, W., Chen, H., Du, K., Asahara, H., Tini, M., Emerson, B.M., Montminy, M. and Evans, R.M. (2001) Science 294, 2507–2551.
[24] Giandomenica, V., Simonsson, M., Grönroons, E. and Ericsson, J. (2003) Mol. Cell. Biol. 23, 2587–2599.